

## Article

# Magnetic and Electronic Properties of Edge-Modified Triangular WS<sub>2</sub> and MoS<sub>2</sub> Quantum Dots

Hazem Abdelsalam<sup>1,2</sup>, Omar H. Abd-Elkader<sup>3,\*</sup> , Nouf S. Zaghloul<sup>4</sup> and Qinfang Zhang<sup>1,\*</sup><sup>1</sup> School of Materials Science and Engineering, Yancheng Institute of Technology, Yancheng 224051, China<sup>2</sup> Theoretical Physics Department, National Research Centre, P.O. Box 21111, Giza 12622, Egypt<sup>3</sup> Department of Physics and Astronomy, College of Science, King Saud University, P.O. Box 2455, Riyadh 11451, Saudi Arabia<sup>4</sup> Bristol Centre for Functional Nanomaterial's, HH Wills Physics Laboratory, Tyndall Avenue, Bristol BS8 1FD, UK

\* Correspondence: omabdelkader7@ksu.edu.sa (O.H.A.-E.); qfangzhang@ycit.edu.cn (Q.Z.)

**Abstract:** The magnetic and electronic properties of zigzag-triangular WS<sub>2</sub> and MoS<sub>2</sub> quantum dots are investigated using density functional theory calculations. The pristine WS<sub>2</sub> and MoS<sub>2</sub> nanodots hold permanent spin on their edges which originates from the unpaired electrons of the transition metals at the edges. The ferromagnetic spin ordering in zigzag-triangular WS<sub>2</sub> and MoS<sub>2</sub> can be transformed to antiferromagnetic ordering with  $S = 0$  and to nonmagnetic, respectively, by edge passivation with 2H. The calculations of the Curie Temperature indicate that these magnetic states are stable and withstand room temperature. The paramagnetic susceptibility of these structures significantly decreases by edge sulfuration. Moreover, it can be converted to diamagnetic susceptibility by edge passivation with 2H as found in WS<sub>2</sub> nanodots. These structures are semiconductors with energy gaps of  $\sim 3.3$  eV that decrease unexpectedly by edge passivation due to the existence of lone pairs from S atoms that give a high contribution to the low-energy molecular orbitals. With these preferable magnetic properties and controlled electronic ones, WS<sub>2</sub> and MoS<sub>2</sub> quantum dots are potential candidates for spintronic applications.

**Keywords:** WS<sub>2</sub> and MoS<sub>2</sub> quantum dots; DFT; magnetic and electronic properties; magnetic susceptibility; spintronics



**Citation:** Abdelsalam, H.; Abd-Elkader, O.H.; Zaghloul, N.S.; Zhang, Q. Magnetic and Electronic Properties of Edge-Modified Triangular WS<sub>2</sub> and MoS<sub>2</sub> Quantum Dots. *Crystals* **2023**, *13*, 251. <https://doi.org/10.3390/cryst13020251>

Academic Editor: Arcady Zhukov

Received: 6 January 2023

Revised: 26 January 2023

Accepted: 30 January 2023

Published: 1 February 2023



**Copyright:** © 2023 by the authors. Licensee MDPI, Basel, Switzerland. This article is an open access article distributed under the terms and conditions of the Creative Commons Attribution (CC BY) license (<https://creativecommons.org/licenses/by/4.0/>).

## 1. Introduction

Two-dimensional quantum dots (2DQDs) are finite nanostructures from single- or few-layer 2D materials with small sizes ranging from 2–10 nm [1,2]. 2DQDs are characterized by many interesting physical and chemical properties such as quantum confinement, edge effect, and ultimate surface areas [3–6]. Based on the tunable electronic properties, 2DQDs found their way toward different applications including transistors [4,7], memory devices [8,9], light-emitting diodes [10,11], and photovoltaic cells [12,13]. The edge effect appearing in 2DQDs due to the small size and the high surface area that can be chemically functionalized makes 2DQDs promising for sensors [14,15], catalysts [16,17], water treatment [18,19], and biological applications [20,21].

Among the family of 2D materials, 2D transition metals dichalcogenides (TMDs) and their corresponding quantum dots show promising characteristics such as sizable band gap [22], near unity quantum yield [23], and strong light absorption [24,25]. For instance, Bastonero et al. reported that vertical heterostructures from PdS<sub>2</sub> and PtS<sub>2</sub> have outstanding light absorption up to 50% in the visible spectrum with a maximum short-circuit current equals to 7.2 mA/cm<sup>2</sup> under solar irradiation. In addition, charge separation between the two layers has been achieved, thus they are ideal applicants for building highly efficient and ultrathin heterojunction solar cells [25].

In the field of spintronics, 2D materials and their quantum dots show interesting properties such as the large spin-orbit coupling in TMDs [26–28] and the intrinsic spin of triangular graphene QDs [29–32]. The origin of the ferromagnetic ground state in triangular graphene or silicene QDs with zigzag edges is the frustrated  $\pi$ -electrons at the edges that cannot form  $\pi$ -bonds with neighbor C or Si atoms due to sublattice imbalance. Thus, they form half-filled electronic states with nonzero net spin; this net spin increases by increasing the size of the triangular QDs. Additional manipulation of the magnetic states of these nanostructures was achieved by connecting these triangular nanodots [33–35]. For example, Mishra et al. fabricated a one-dimensional spin chain using triangular graphene having  $S = 1$  as the building blocks [35]. In this antiferromagnetic  $S = 1$  chain, gapped spin excitations in the bulk and gapless fractional excitations,  $S = 1/2$ , at the chain termination were observed [36,37].

In this work, we study the magnetic properties of triangular MoS<sub>2</sub> and WS<sub>2</sub> quantum dots with zigzag termination. The goal of this work is to study the combined effect of both the zigzag edges, which created non-zero spin in nanographene and the intrinsic magnetism by the d-orbitals of the transition metals on the magnetic properties of the selected nanostructures. Moreover, we investigate the effect of edge modification on the magnetic and electronic properties by considering pristine edges and edge passivation with 2H and S atoms. These effects show interesting properties such as control over the spin-polarized ground state and magnetic susceptibility. It is worth noting that Bertel et al. and Tiutiunyk et al. have recently investigated the electronic, optical, and magnetic properties of triangular MoS<sub>2</sub> quantum dots using DFT calculations [38,39]. The total magnetic moment was used as an indicator for studying the magnetic properties. The main difference between our works is that they focus on the effects of doping and size on the properties while we consider different edge morphology and chemical functionalization of the edges that facilitates precise control over the magnetic and electronic properties. We also studied the magnetic susceptibility which has not been studied before for these nanodots. The magnetic susceptibility investigations show that the considered nanodots can be converted from paramagnetic to diamagnetic by passivating the transition metals on the edges with 2H or S atoms. The paper is organized as follows: the computational model is given in Section 2, the results and the discussion are presented in Section 3, the conclusion is provided in Section 4, and finally, the supporting materials are given in Appendix A.

## 2. Computational Model

The magnetic and electronic properties of the selected TMDs are investigated using DFT calculations as implemented in Gaussian 16 [40]. The calculations were made using the hybrid M062X functional [41] and the effective core potential LANL2DZ basis set [42]. This level of theory shows accuracy and adequacy for calculations of transition metals-based compounds and similar systems [43–45]. The magnetic ordering is specified by optimizing the structure at different magnetic states, namely closed shell (nonmagnetic), open shell (antiferromagnetic ordering), and various spin-polarized states. The state with the lowest total energy is chosen as the ground state of the structure. Since calculations of spin-polarized states (triplet, quintet, etc.) are complicated and require high computational power, thus we optimize the structures using a self-consistent field (SCF) convergence criterion of  $10^{-4}$ . However, to test the considered order of convergence, we performed one set of runs for the different magnetic states of T-MoS<sub>2</sub> with conversion criterion of  $10^{-7}$ . We found that in both cases the magnetic state with the lowest ground state energy is the same in both cases, namely the septet spin state. Additionally, the difference between the ground state energy in the two cases is only 0.004 eV. Therefore, the approximated conversion used here can be considered reasonable when considering both computational power and results accuracy.

### 3. Results and Discussion

The triangular quantum dots considered in this work are shown in Figure 1 for WS<sub>2</sub>, the same structures are also considered for MoS<sub>2</sub>. Figure 1a represents triangular WS<sub>2</sub> (T-WS<sub>2</sub>) in the pristine case, without any edge passivation. This nanodot is then passivated by attaching sulfur/2H atoms to the edge transition metals, as shown in Figure 1b,c. Another morphology of the edges, with more transition metal at the edges, is considered in Figure 1c,d for the pristine edges and the sulfurated ones.

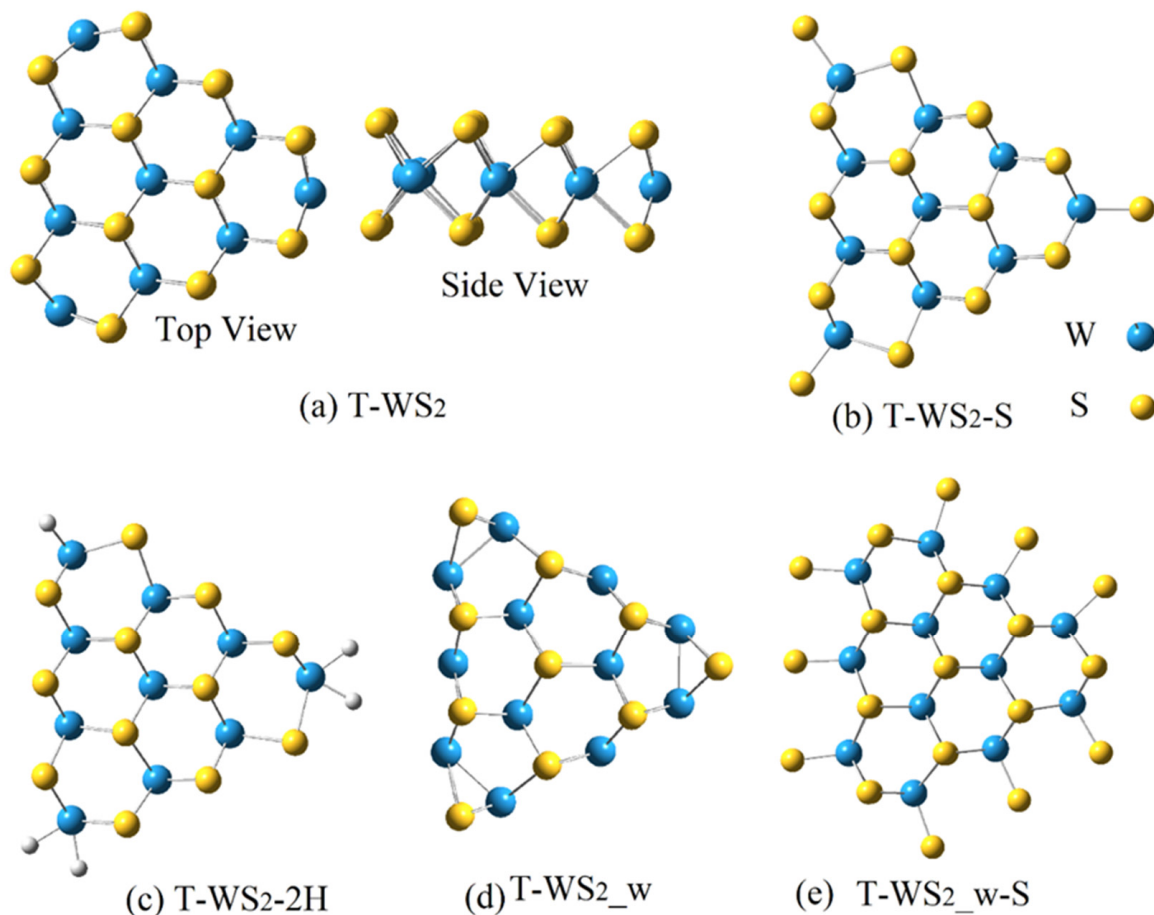


**Figure 1.** Optimized structures of triangular WS<sub>2</sub> with pristine (a), sulfurated (b), and double hydrogenated edges (c). The structures in (d,e) represent pristine and sulfurated WS<sub>2</sub> using another way of building the triangular structure to increase the number of edge Mo atoms.

#### 3.1. Structure Stability

The stability of the considered WS<sub>2</sub> and MoS<sub>2</sub> quantum dots are investigated by two means. First, we calculated the binding energy ( $E_b$ ) using the following equation:

$$E_b = (n_m E_m + n_s E_s + n_H E_H - E_t) / n_t \quad (1)$$

where  $n_m$ ,  $n_s$ ,  $n_H$ , and  $n_t$  are the number of transition metals, sulfur, hydrogen, and the total number of atoms, respectively.  $E_m$ ,  $E_s$ ,  $E_H$ , and  $E_t$  are the corresponding energies. As given in Table 1, the binding energy has values from 5.1 to 5.9 eV. The pristine quantum dots, especially those with a higher number of transition metals at the edges, have slightly higher binding energy, which is a result of the edge reconstruction and the formation of stronger bonds between the metal atoms compared to the bonds between metals and passivating elements. In general, all the binding energy values are positive, which ensures the stable formation of these quantum dots from their constituent elements. Frequency calculations are the second tool that we used to test the stability of the considered structures. From

frequency calculations, we can obtain the infrared (IR) spectrum which holds detailed information about the structure and its dynamics. The IR spectrum is a relation between the vibrational frequencies and the corresponding transition intensity. If the vibrational frequencies are positive this means that the structure is in its ground state. While negative frequencies in the IR spectrum are an indicator of a nonoptimized, transition state, or unstable structure. According to the IR spectra shown in Figure A1 (Appendix A) for the investigated structures, all the vibrational frequencies are positive which confirms that the structures are in their fully relaxed ground states, and are consequently, dynamically stable.

**Table 1.** The binding energy ( $E_b$ ), magnetic state (MS), spin (S), and the modules of the difference between the antiferromagnetic ground state energy and the ferromagnetic ground state energy ( $\Delta E$ ). The last three columns give Curie Temperature ( $T_C$ ), the magnetic susceptibility ( $\chi_m$ ), and the energy gap ( $E_g$ ).

Struct.	$E_b$	MS	S	$\Delta E$ (eV)	$T_C$ (K)	$\chi_m$ (a.u)	$E_g$ (eV)
T-WS <sub>2</sub>	5.57	Sept	3	0.25	645	57.64	$E_{g\alpha} = 3.39, E_{g\beta} = 3.39$
T-WS <sub>2</sub> -S	5.59	Trp	1	0.29	748	53.67	$E_{g\alpha} = 3.47, E_{g\beta} = 2.65$
T-WS <sub>2</sub> -2H	5.14	Opn	0	1.26	3294	-22.37	$E_{g\alpha} = 2.53, E_{g\beta} = 2.53$
T-WS <sub>2</sub> -w	5.78	Sept	3	1.36	1169	160.12	$E_{g\alpha} = 2.57, E_{g\beta} = 2.83$
T-WS <sub>2</sub> -w-S	5.78	cls	0	—	—	-16.40	$E_g = 3.19$
T-MoS <sub>2</sub>	5.56	Nont	4	0.021	54	67.27	$E_{g\alpha} = 2.47, E_{g\beta} = 3.39$
T-MoS <sub>2</sub> -S	5.54	Trp	1	1.03	2656	17.42	$E_{g\alpha} = 3.46, E_{g\beta} = 2.93$
T-MoS <sub>2</sub> -2H	5.06	cls	0	—	—	66.59	$E_g = 2.78$
T-MoS <sub>2</sub> -Mo	5.91	Nont	4	1.81	1556	645.80	$E_{g\alpha} = 3.22, E_{g\beta} = 3.53$
T-MoS <sub>2</sub> -Mo-S	5.75	Trp	1	0.29	748	137.69	$E_{g\alpha} = 3.14, E_{g\beta} = 3.29$

### 3.2. Magnetic Properties

The magnetic state (MS) is obtained by calculating the optimized ground states energy for nonmagnetic and magnetic initial states, the one with the lowest ground state energy is defined as the magnetic state of the structure. In Table 1, For instance, the MS of the pristine triangular WS<sub>2</sub> (T-WS<sub>2</sub>) is the septet state (sept in Table 1) while the sulfurated one (T-WS<sub>2</sub>-S) is the triplet state (trp). This means that the net spin of T-WS<sub>2</sub> decreases from  $S = 3$  to  $S = 1$  by edge sulfuration as shown for T-WS<sub>2</sub>-S. Further decrease of the net spin to the antiferromagnetic spin ordering with  $S = 0$  can be obtained by passivating edge W atoms with 2H atoms, see TWS<sub>2</sub>-2H in Table 1. The interesting case of T-WS<sub>2</sub>-w (shown in Figure 1d) that has ferromagnetic ordering with  $S = 3$  can be converted to the nonmagnetic ordering by edge sulfuration as given in Table 1. Thus, the net value of the spin and its ordering in triangular WS<sub>2</sub> are strongly affected by the terminating edge atoms and their passivation.

The origin of the spin is the unpaired electrons in the d-orbital of the transition metal. Since the hybridization of WS<sub>2</sub> or MoS<sub>2</sub> is the  $sd^5$  hybridization, then every transition metal should be bound to six neighbor atoms. Decreasing the number of surrounding S atoms by any means, such as S-vacancy at the surface or the edges of QDs as in our case, will create frustrated electrons unable to bind with neighbor atoms and eventually form half-filled electronic states. As seen in Figure 1a, T-WS<sub>2</sub> has three W atoms at the edges that form only four bonds with neighbor S atoms. Therefore, T-WS<sub>2</sub> will have six unpaired electrons that form the septet spin state with  $S = 3$ . This result is confirmed by the spin distribution shown in Figure 2a where the spin density, mainly contributed to by the spin-up density, is localized on the edge W atoms. Attaching 2H atoms to the edge W atoms will passivate their frustrated electrons and form the antiferromagnetic ordering with  $S = 0$ . Passivation with atoms having two unpaired electrons such as S atoms in T-WS<sub>2</sub>-S does not passivate the two unpaired electrons of the W atoms at the edges as the 2H did because the  $sp^3$  hybridization of S atoms requires a specific bond angle between all the hybrid orbitals. Thus, an S atom passivates only one electron from the edge W atom which eventually

leaves three unpaired electrons in S atoms and three in Mo atoms that interact together and make the structure have a final spin triplet state with  $S = 1$ .

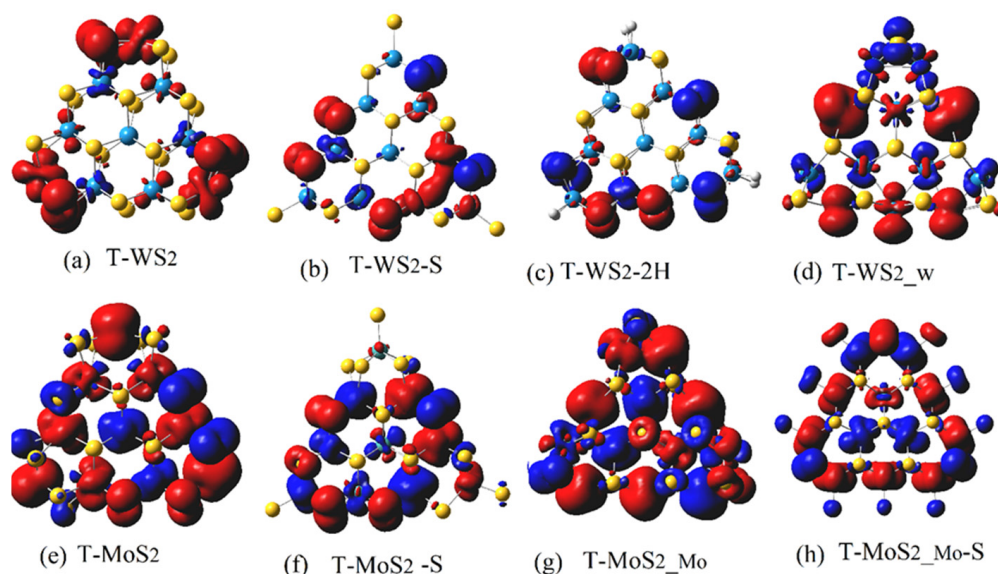


**Figure 2.** Spin density distribution of spin up (red) and spin down (blue) on  $\text{WS}_2$  and  $\text{MoS}_2$  quantum dots before and after double hydrogenation as labeled below each subfigure, the isovalue of the spin density is  $0.004 \text{ \AA}^{-3}$ .

The structure  $\text{T-WS}_2\text{-w}$  is expected to have a higher value of spin due to the higher number of W atoms at the edges. However, this does not happen and the net spin is 3, similar to the  $\text{T-WS}_2$  as given in Table 1. As seen in Figure 1d, the majority of the edge W atoms are already passivated by interacting with each other, thus they do not participate in the net spin. The ferromagnetic spin ordering of  $\text{T-WS}_2\text{-w}$  can be transformed to antiferromagnetic ordering with  $S = 0$  by edge sulfuration, see Figure 1e, where the unpaired two electrons from S atoms passivate the unpaired ones from W atoms. The magnetic ordering of  $\text{T-MoS}_2$  and its derivatives should, in general, have the same behavior as  $\text{T-WS}_2$  because they have the same orbital hybridization and the same number of electrons participating in the bonds between the transition metal and the chalcogen that form the monolayer TMDs. However, the deformation, which is higher in  $\text{MoS}_2$  quantum dots, increases the net spin in some cases such as the nonet spin state in  $\text{T-MoS}_2$ . The enhanced spin in  $\text{T-MoS}_2$  compared to  $\text{T-WS}_2$  can be seen in Figure 2e where the spin density distributes not only on the transition metal at the edge but also on the surface atoms. The net spin in  $\text{T-MoS}_2$  is controlled by edge passivation similar to  $\text{T-WS}_2$ , where passivation with S atoms lowers the spin state to the triplet state and passivation with 2H results in  $S = 0$  and antiferromagnetic spin ordering.

The magnetic stability is investigated by calculating the ground state energy difference between the antiferromagnetic spin state and the ferromagnetic one ( $\Delta E$ ).  $\Delta E$  is then used to estimate the Curie temperature ( $T_C$ ) based on the mean-field theory using the following equation [46,47]:

$$T_C = 2\Delta E / (3c \cdot k_B) \quad (2)$$

where  $c$  is the number of magnetic atoms; here it is the transition metal at the edges, and  $k_B$  is the Boltzmann constant. The obtained values of  $\Delta E$  and  $T_C$  are given in Table 1, it is observed that all the structures, except  $\text{T-MoS}_2$ , have a Curie temperature higher than room temperature. These results indicate that the magnetic states of the considered nanodots are stable and withstand room temperature.

The magnetic properties considered previously account only for the effect of edges on the magnetic state of the structure. However, for a complete description of the type of the material, whether it is diamagnetic, paramagnetic, or ferromagnetic, we need to include all

electrons interacting with the magnetic field. This can be done by calculating the magnetic susceptibility ( $\chi_m$ ). It is defined as the second derivate of the ground state energy ( $E$ ) with respect to the applied magnetic field ( $B$ ):

$$\chi_m = \mu_0 \frac{d^2 E}{d^2 B^2} \quad (3)$$

where  $\mu_0$  is the vacuum permeability [48]. The calculations are done using the GIAO method which requires lower computational power compared to other methods such as CSGT [49]. The  $\chi_m$  given in Table 1 is the sum of isotropic diamagnetic susceptibility (negative) and isotropic paramagnetic susceptibility (positive). Thus, a positive/negative value of the total susceptibility means that the material is paramagnetic/diamagnetic. It is observed from Table 1 that both T-WS<sub>2</sub> and T-MoS<sub>2</sub> are paramagnetic with positive  $\chi_m$ . The value of  $\chi_m$  significantly affected by edge sulfuration or hydrogenation. Attaching sulfur atoms to the edge W or Mo atoms decreases the paramagnetism, for instance in T-MoS<sub>2</sub> the magnetic susceptibility decreases from ~67 (a.u.) to 17 (a.u). Moreover, the paramagnetic T-WS<sub>2</sub> can be transformed into diamagnetic material by double hydrogenation where  $\chi_m$  equals −22.4 (a.u) for T-WS<sub>2</sub>-2H as given in Table 1. The highest value of  $\chi_m$  was observed for T-MoS<sub>2</sub>\_Mo, which is mainly due to the higher number of non-passivated Mo atoms at the edges. The same was also found in T-WS<sub>2</sub>. Thus, the paramagnetism/diamagnetism of TMDs quantum dots can be controlled by the number of unpassivated/passivated transition metals. Further control over the magnetic properties can be achieved by the lateral or vertical connection of these nanodots similar to the lateral connection of graphene quantum dots [35]. These 2D heterostructures are expected to be an interesting research point for future work to study the type of coupling between the quantum dots, whether it is ferromagnetic or antiferromagnetic coupling. For this task, it is more accurate to use the broken symmetry-DFT approach for describing these complex systems [50–52].

### 3.3. Electronic Properties

From the last column in Table 1 which gives the values of the energy gaps, we started the discussion of the electronic properties of the selected TMDs quantum dots. The energy gap ( $E_g$ ) is given by,  $E_g = E_{\text{LUMO}} - E_{\text{HOMO}}$  where  $E_{\text{LUMO}}$  is the energy of the lowest unoccupied molecular orbital and  $E_{\text{HOMO}}$  is the energy of the highest occupied molecular orbital. The energy gaps show that T-WS<sub>2</sub> and T-MoS<sub>2</sub> are semiconductors with spin-up energy gaps ( $E_{g\alpha}$ ) of ~3.4 eV and 2.47 eV, respectively, and spin-down energy gap ( $E_{g\beta}$ ) of ~3.4 eV. These energy gaps are relatively high when compared to the energy gaps of a single layer, where the energy gaps of WS<sub>2</sub> and MoS<sub>2</sub> monolayers equal 2.03 and 1.88 eV, respectively [53]. This increase in the energy gaps of the quantum dots is mainly a result of the quantum confinement effect, where decreasing the size leads to an increase in the energy gap. The spin-up energy gap of T-WS<sub>2</sub> is almost unaffected by edge sulfuration or hydrogenation, while the spin-down energy gap decreases to 2.7 eV and 2.01 eV in T-WS<sub>2</sub>-S and T-WS<sub>2</sub>-2H, respectively. The energy gaps strongly decrease to  $E_{g\alpha} = 2.57$  and  $E_{g\beta} = 2.83$  eV in T-WS<sub>2</sub>\_w due to the higher number of unpassivated W atoms at the edges. The same behavior is observed in T-MoS<sub>2</sub> after passivation with the lowest energy gap equal to 2.78 eV in T-MoS<sub>2</sub>-2H. The changes in the energy gap can be understood by considering the low-energy molecular orbitals and their distribution, namely the highest occupied molecular orbital (HOMO) and lowest unoccupied molecular orbital (LUMO) as seen in Figure 3.

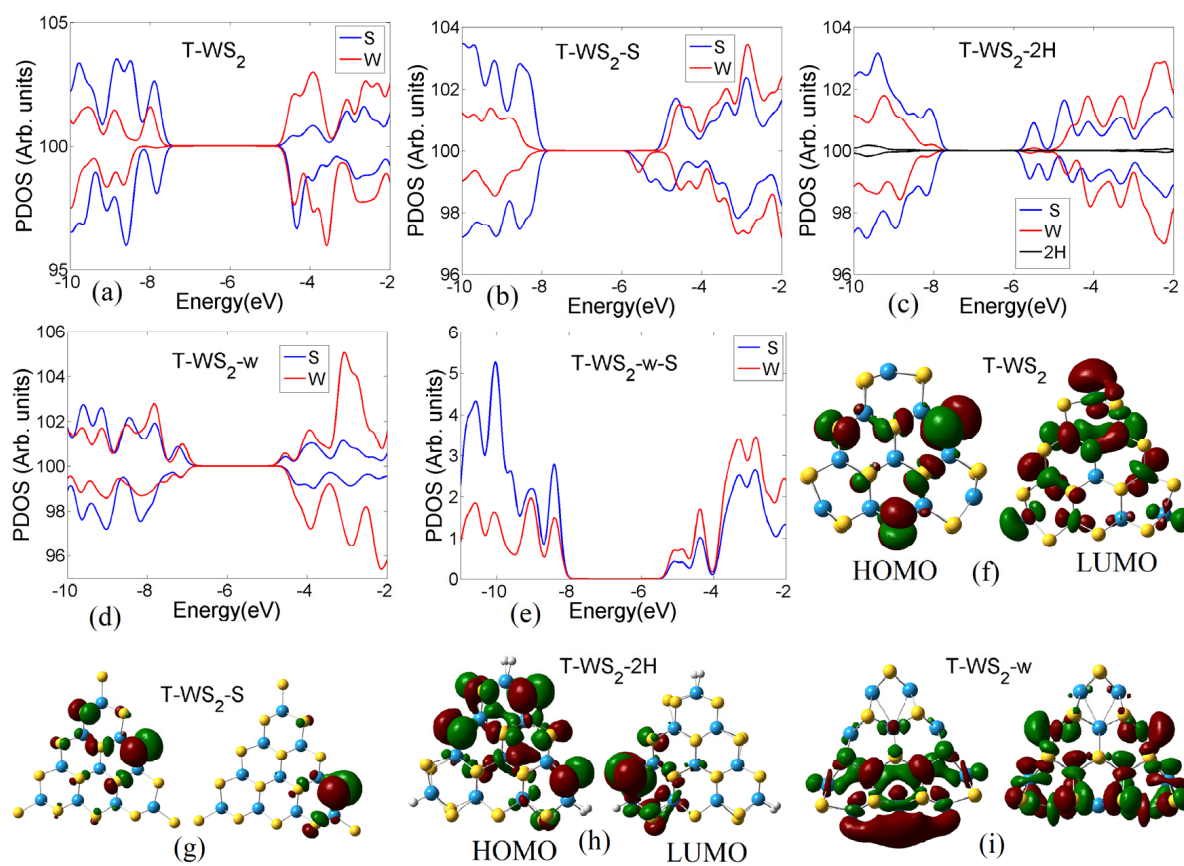


**Figure 3.** (a–e) Electronic partial density of states of T-WS<sub>2</sub> with and without edge passivation. (f–i) The corresponding HOMO/LUMO distributions for spin-up molecular orbitals. The red and green colors in (f–i) represent the positive and negative phase distribution in the molecular orbital wave function, respectively.

The partial density of states (PDOS) of T-WS<sub>2</sub> in Figure 3a shows that the spin-up HOMO (LUMO) peaks originate mainly from sulfur (S) atoms. This means that the electron lone pairs in sulfur have lower energy than the unpaired electrons from W atoms. This is confirmed by the distribution of HOMO on sulfur atoms and the LUMO on W atoms, as seen in Figure 3f. For the spin-down case, the HOMO and LUMO are mainly from sulfur atoms. After passivation with S or 2H, the contribution of W atoms to the HOMO and LUMO significantly decreases due to the passivation of their unpaired electrons to form stronger bonds deeper in the valance band. In this case, the HOMO and LUMO distribute on S atoms as seen in Figure 3g,h. The decrease in the energy gap is a result of the shifting of the LUMO toward the HOMO as seen in Figure 3b,c. The contribution of W atoms to the low energy orbitals significantly increases in T-WS<sub>2</sub>-w, Figure 3d,i, due to the higher number of W atoms at the edges.

The partial densities of states of T-MoS<sub>2</sub> with different edge terminations are shown in Figure 4, from which we can identify the contribution of sulfur and molybdenum atoms to the low-energy molecular orbitals. Similar to T-WS<sub>2</sub>, it is noted that the sulfur atoms provide a higher contribution to the low energy levels than the Mo atoms, except for the case in Figure 4d due to the higher number of Mo atoms at the edges. Thus, the interactions of the WS<sub>2</sub> or MoS<sub>2</sub> quantum dots with other materials can be controlled to be through the transition metal or the chalcogen by controlling the edge type. Regarding prospective work on 2D heterostructures based on these nanodots, it is expected that these heterostructures will provide great control of the electronic properties of these systems. For example, the formation of 2D heterojunctions with tunable electronic and magnetic properties applicable to different electronic and photovoltaic applications.

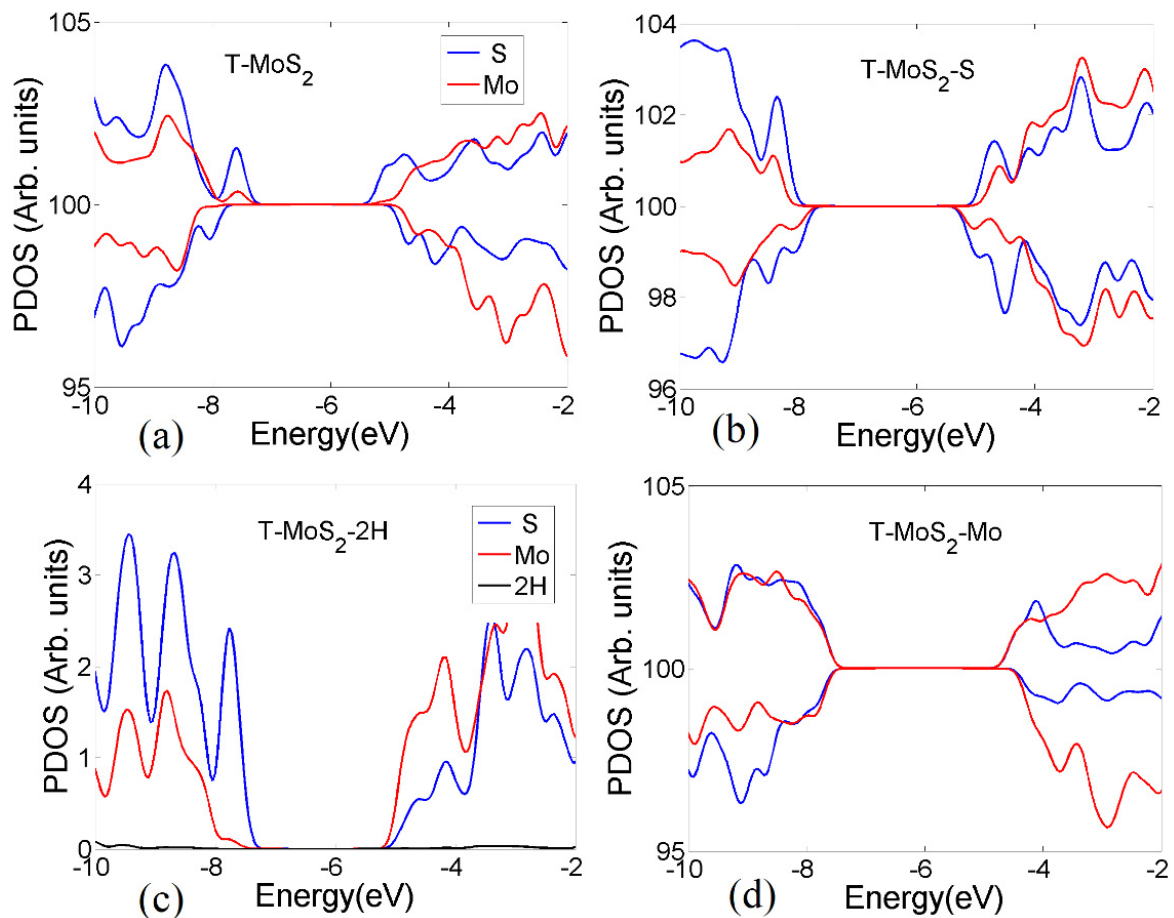


**Figure 4.** Electronic density of states of T-MoS<sub>2</sub> before (a,d) and after (b,c) edge passivation with S and 2H.

#### 4. Conclusions

The magnetic and electronic properties of triangular WS<sub>2</sub> (T-WS<sub>2</sub>) and MoS<sub>2</sub> (T-MoS<sub>2</sub>) quantum dots are investigated using density functional theory calculations. The optimization process was performed for different magnetic states, namely closed-shell (nonmagnetic), open-shell (magnetic with antiferromagnetic ordering), and spin-polarized states. In the pristine case, both the triangular WS<sub>2</sub> and MoS<sub>2</sub> have ferromagnetic ordering with net spin equal to 3 and 4, respectively. The origin of the spin is the unpaired d-orbital electrons from the W or Mo atoms at the edges. Attaching S or 2H atoms to the transition metals at the edges significantly decreases the net spin due to the passivation of their unpaired electrons. For instance, the net spin that equals 3 in T-WS<sub>2</sub> decreases to zero with antiferromagnetic ordering after passivation with 2H. Additionally, T-MoS<sub>2</sub> with S = 4 transforms to nonmagnetic by passivation with 2H. The calculated Curie temperatures show that the obtained magnetic states are stable and detectable at room temperature and higher. The considered nanodots are paramagnetic with positive magnetic susceptibility. Increasing the number of sulfur atoms by edge sulfuration decreases the magnetic susceptibility and, in some cases, converts the structure to diamagnetic with negative susceptibility. The electronic density of states shows that MoS<sub>2</sub> and WS<sub>2</sub> quantum dots are semiconductors with a wide energy gap of ~3.3 eV that is slightly decreased by edge passivation. The unexpected decrease is a result of the lone pairs from the S atoms at the edges that participate in the low-energy orbitals. Thus, edge passivation is an effective tool that can tune the electronic and magnetic properties of transition metal dichalcogenides quantum dots.

**Author Contributions:** Conceptualization, H.A.; methodology, H.A. and Q.Z.; software, Q.Z.; validation, H.A.; formal analysis, O.H.A.-E.; investigation, H.A.; resources, O.H.A.-E.; data curation, H.A.; writing—original draft preparation, O.H.A.-E., N.S.Z. and H.A.; writing—review and editing, O.H.A.-E. and Q.Z.; visualization, O.H.A.-E., N.S.Z. and H.A.; supervision, O.H.A.-E. and Q.Z.; project administration, O.H.A.-E. and H.A.; funding acquisition, O.H.A.-E. and Q.Z. All authors have read and agreed to the published version of the manuscript.

**Funding:** This work is supported by the National Natural Science Foundation of China (No. 12274361), the Ministry of Science and Technology, Foreign Experts Program (No. QN2021014007L, QN2022014009L), and the Natural Science Foundation of Jiangsu Province (BK20211361, 20KJA430004). This work is supported also by Researchers Supporting Project number (RSP2023R468), King Saud University, Riyadh, Saudi Arabia.

**Data Availability Statement:** The data presented in this study are available on request from the corresponding authors.

**Conflicts of Interest:** There is no conflict of interest to declare.

## Appendix A

Figure A1 shows the infrared spectra (IR) of MoS<sub>2</sub> and WS<sub>2</sub> quantum dots. It is observed that all the IR intensity peaks occur at a positive vibrational frequency which confirms the geometrical stability of the considered structures.

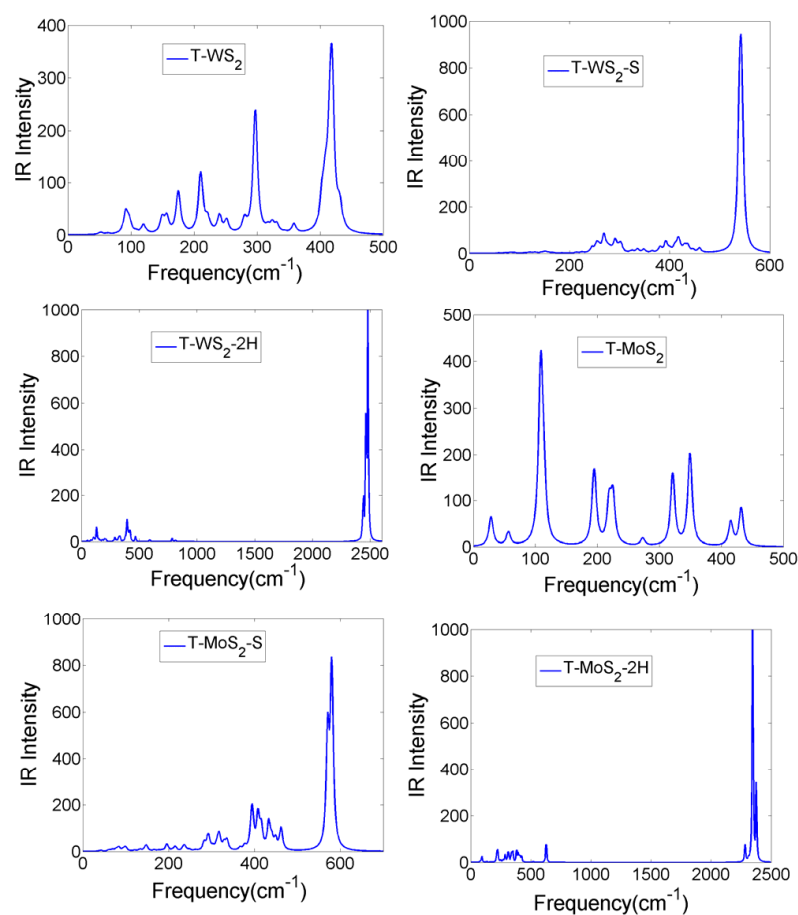


**Figure A1.** Infrared spectra of selected WS<sub>2</sub> and MoS<sub>2</sub> quantum dots before and after edge passivation.

## References

1. Wang, X.; Sun, G.; Li, N.; Chen, P. Quantum dots derived from two-dimensional materials and their applications for catalysis and energy. *Chem. Soc. Rev.* **2016**, *45*, 2239–2262. [[CrossRef](#)] [[PubMed](#)]
2. Abdelsalam, H.; Zhang, Q.F. Properties and applications of quantum dots derived from two-dimensional materials. *Adv. Phys. X* **2022**, *7*, 2048966. [[CrossRef](#)]
3. Ramalingam, G.; Kathirgamanathan, P.; Ravi, G.; Elangovan, T.; Kumar, B.A.; Manivannan, N.; Kasinathan, K. Quantum Confinement Effect of 2D Nanomaterials. In *Quantum Dots—Fundamental and Applications*; IntechOpen: London, UK, 2020; pp. 1–12. [[CrossRef](#)]
4. Ponomarenko, L.A.; Schedin, F.; Katsnelson, M.I.; Yang, R.; Hill, E.W.; Novoselov, K.S.; Geim, A.K. Chaotic Dirac Billiard in Graphene Quantum Dots. *Science* **2008**, *320*, 356–358. [[CrossRef](#)] [[PubMed](#)]
5. Cao, Y.; Dong, H.; Pu, S.; Zhang, X. Photoluminescent two-dimensional SiC quantum dots for cellular imaging and transport. *Nano Res.* **2018**, *11*, 4074–4081. [[CrossRef](#)]
6. Biswas, M.C.; Islam, T.; Nandy, P.K.; Hossain, M. Graphene Quantum Dots (GQDs) for Bioimaging and Drug Delivery Applications: A Review. *ACS Mater. Lett.* **2021**, *3*, 889–911. [[CrossRef](#)]
7. Liu, Y.; Duan, X.; Shin, H.-J.; Park, S.; Huang, Y.; Duan, X. Promises and prospects of two-dimensional transistors. *Nature* **2021**, *591*, 43–53. [[CrossRef](#)]
8. Han, S.-T.; Hu, L.; Wang, X.; Zhou, Y.; Zeng, Y.-J.; Ruan, S.; Pan, C.; Peng, Z. Black Phosphorus Quantum Dots with Tunable Memory Properties and Multilevel Resistive Switching Characteristics. *Adv. Sci.* **2017**, *4*, 1600435. [[CrossRef](#)]
9. Lv, Z.; Wang, Y.; Chen, J.; Wang, J.; Zhou, Y.; Han, S.-T. Semiconductor Quantum Dots for Memories and Neuromorphic Computing Systems. *Chem. Rev.* **2020**, *120*, 3941–4006. [[CrossRef](#)]
10. Palacios-Berraquero, C. Atomically-thin quantum light emitting diodes. In *Quantum Confined Excitons in 2-Dimensional Materials*; Springer: Cham, Switzerland, 2018; pp. 71–89.
11. Aharonovich, I.; Englund, D.; Toth, M. Solid-state single-photon emitters. *Nat. Photonics* **2016**, *10*, 631–641. [[CrossRef](#)]
12. Abdelsalam, H.; Atta, M.M.; Osman, W.; Zhang, Q. Two-dimensional quantum dots for highly efficient heterojunction solar cells. *J. Colloid Interface Sci.* **2021**, *603*, 48–57. [[CrossRef](#)]
13. Najafi, L.; Taheri, B.; Martín-García, B.; Bellani, S.; Di Girolamo, D.; Agresti, A.; Oropesa-Núñez, R.; Pescetelli, S.; Vesce, L.; Calabrò, E.; et al. MoS<sub>2</sub> Quantum Dot/Graphene Hybrids for Advanced Interface Engineering of a CH<sub>3</sub>NH<sub>3</sub>PbI<sub>3</sub> Perovskite Solar Cell with an Efficiency of over 20%. *ACS Nano* **2018**, *12*, 10736–10754. [[CrossRef](#)] [[PubMed](#)]
14. Ghazi, M.; Janfaza, S.; Tahmooressi, H.; Ravishankara, A.; Earl, E.; Tasnim, N.; Hoorfar, M. Enhanced selectivity of microfluidic gas sensors by modifying microchannel geometry and surface chemistry with graphene quantum dots. *Sens. Actuators B Chem.* **2021**, *342*, 130050. [[CrossRef](#)]
15. Abdelsalam, H.; Saroka, V.A.; Atta, M.M.; Abd-Elkader, O.H.; Zaghloul, N.S.; Zhang, Q. Tunable Sensing and Transport Properties of Doped Hexagonal Boron Nitride Quantum Dots for Efficient Gas Sensors. *Crystals* **2022**, *12*, 1684. [[CrossRef](#)]
16. Liu, Y.; Zhang, W.; Zheng, W. Quantum Dots Compete at the Acme of MXene Family for the Optimal Catalysis. *Nano-Micro Lett.* **2022**, *14*, 158. [[CrossRef](#)] [[PubMed](#)]
17. Osman, W.; Saad, M.A.; Ibrahim, M.A.; Yahia, I.S.; Abdelsalam, H.; Zhang, Q. Electronic, optical, and catalytic properties of finite antimonene nanoribbons: First principles study. *Phys. Scr.* **2022**, *97*, 035802. [[CrossRef](#)]
18. Abdelsalam, H.; Younis, W.O.; Saroka, V.A.; Teleb, N.H.; Yunoki, S.; Zhang, Q. Interaction of hydrated metals with chemically modified hexagonal boron nitride quantum dots: Wastewater treatment and water splitting. *Phys. Chem. Chem. Phys.* **2020**, *22*, 2566–2579. [[CrossRef](#)]
19. Sivaranjani, P.; Janani, B.; Thomas, A.M.; Raju, L.L.; Khan, S.S. Recent development in MoS<sub>2</sub>-based nano-photocatalyst for the degradation of pharmaceutically active compounds. *J. Clean. Prod.* **2022**, *352*, 131506. [[CrossRef](#)]
20. Iravani, S.; Varma, R.S. Smart MXene Quantum Dot-Based Nanosystems for Biomedical Applications. *Nanomaterials* **2022**, *12*, 1200. [[CrossRef](#)]
21. Niu, Y.; Li, J.; Gao, J.; Ouyang, X.; Cai, L.; Xu, Q. Two-dimensional quantum dots for biological applications. *Nano Res.* **2021**, *14*, 3820–3839. [[CrossRef](#)]
22. Wang, Q.H.; Kalantar-Zadeh, K.; Kis, A.; Coleman, J.N.; Strano, M.S. Electronics and optoelectronics of two-dimensional transition metal dichalcogenides. *Nat. Nanotechnol.* **2012**, *7*, 699–712. [[CrossRef](#)]
23. Amani, M.; Lien, D.-H.; Kiriya, D.; Xiao, J.; Azcatl, A.; Noh, J.; Madhupathy, S.R.; Addou, R.; Kc, S.; Dubey, M.; et al. Near-unity photoluminescence quantum yield in MoS<sub>2</sub>. *Science* **2015**, *350*, 1065–1068. [[CrossRef](#)] [[PubMed](#)]
24. Bahauddin, S.M.; Robotjazi, H.; Thomann, I. Broadband Absorption Engineering to Enhance Light Absorption in Monolayer MoS<sub>2</sub>. *ACS Photonics* **2016**, *3*, 853–862. [[CrossRef](#)]
25. Bastonero, L.; Cicero, G.; Palummo, M.; Fiorentin, M.R. Boosted Solar Light Absorbance in PdS<sub>2</sub>/PtS<sub>2</sub> Vertical Heterostructures for Ultrathin Photovoltaic Devices. *ACS Appl. Mater. Interfaces* **2021**, *13*, 43615–43621. [[CrossRef](#)] [[PubMed](#)]
26. Zhu, Z.Y.; Cheng, Y.C.; Schwingenschlögl, U. Giant spin-orbit-induced spin splitting in two-dimensional transition-metal dichalcogenide semiconductors. *Phys. Rev. B* **2011**, *84*, 153402. [[CrossRef](#)]
27. Wakamura, T.; Reale, F.; Palczynski, P.; Zhao, M.Q.; Johnson, A.T.C.; Guéron, S.; Mattevi, C.; Ouerghi, A.; Bouchiat, H. Spin-orbit interaction induced in graphene by transition metal dichalcogenides. *Phys. Rev. B* **2019**, *99*, 245402. [[CrossRef](#)]

28. Husain, S.; Gupta, R.; Kumar, A.; Kumar, P.; Behera, N.; Brucas, R.; Chaudhary, S.; Svedlindh, P. Emergence of spin–orbit torques in 2D transition metal dichalcogenides: A status update. *Appl. Phys. Rev.* **2020**, *7*, 041312. [[CrossRef](#)]
29. Osman, W.; Abdelsalam, H.; Ali, M.; Tebeb, N.; Yahia, I.; Ibrahim, M.; Zhang, Q. Electronic and magnetic properties of graphene quantum dots doped with alkali metals. *J. Mater. Res. Technol.* **2021**, *11*, 1517–1533. [[CrossRef](#)]
30. Su, J.; Telychko, M.; Hu, P.; Macam, G.; Mutombo, P.; Zhang, H.; Bao, Y.; Cheng, F.; Huang, Z.-Q.; Qiu, Z.; et al. Atomically precise bottom-up synthesis of  $\pi$ -extended [5] triangulene. *Sci. Adv.* **2019**, *5*, eaav7717. [[CrossRef](#)]
31. Mishra, S.; Beyer, D.; Eimre, K.; Liu, J.; Berger, R.; Groening, O.; Pignedoli, C.A.; Müllen, K.; Fasel, R.; Feng, X.; et al. Synthesis and Characterization of  $\pi$ -Extended Triangulene. *J. Am. Chem. Soc.* **2019**, *141*, 10621–10625. [[CrossRef](#)]
32. Abdelsalam, H.; Yunoki, S.; Zhang, Q. Boosted spintronic properties in triangular Si-based nanoflakes. *Phys. E Low-Dimens. Syst. Nanostructures* **2021**, *130*, 114699. [[CrossRef](#)]
33. Cheng, S.; Xue, Z.; Li, C.; Liu, Y.; Xiang, L.; Ke, Y.; Yan, K.; Wang, S.; Yu, P. On-surface synthesis of triangulene trimers via dehydration reaction. *Nat. Commun.* **2022**, *13*, 1705. [[CrossRef](#)]
34. Abdelsalam, H.; Atta, M.M.; Saroka, V.A.; Zhang, Q. Anomalous magnetic and transport properties of laterally connected graphene quantum dots. *J. Mater. Sci.* **2022**, *57*, 14356–14370. [[CrossRef](#)]
35. Mishra, S.; Catarina, G.; Wu, F.; Ortiz, R.; Jacob, D.; Eimre, K.; Ma, J.; Pignedoli, C.A.; Feng, X.; Ruffieux, P.; et al. Observation of fractional edge excitations in nanographene spin chains. *Nature* **2021**, *598*, 287–292. [[CrossRef](#)] [[PubMed](#)]
36. Haldane, F.D.M. Nonlinear Field Theory of Large-Spin Heisenberg Antiferromagnets: Semiclassically Quantized Solitons of the One-Dimensional Easy-Axis Néel State. *Phys. Rev. Lett.* **1983**, *50*, 1153–1156. [[CrossRef](#)]
37. Affleck, I. Quantum spin chains and the Haldane gap. *J. Phys. Condens. Matter* **1989**, *1*, 3047–3072. [[CrossRef](#)]
38. Bertel, R.; Mora-Ramos, M.; Correa, J. Electronic properties and optical response of triangular and hexagonal MoS<sub>2</sub> quantum dots. A DFT approach. *Phys. E Low-Dimens. Syst. Nanostructures* **2019**, *109*, 201–208. [[CrossRef](#)]
39. Tiutiunnyk, A.; Morales, A.L.; Bertel, R.; Restrepo, R.L.; Nava-Maldonado, F.M.; Martínez-Orozco, J.C.; Laroze, D.; Duque, C.A.; Correa, J.D.; Mora-Ramos, M.E. Electronic, Optical, and Magnetic Properties of Doped Triangular MoS<sub>2</sub> Quantum Dots: A Density Functional Theory Approach. *Phys. Status Solidi* **2022**, *259*, 2100509. [[CrossRef](#)]
40. Frisch, M.; Trucks, G.; Schlegel, H.; Scuseria, G.; Robb, M.; Cheeseman, J.; Scalmani, G.; Barone, V.; Petersson, G.; Nakatsuji, H.; et al. *Gaussian 16*; Gaussian Inc.: Wallingford, CT, USA, 2016.
41. Zhao, Y.; Truhlar, D.G. The M06 suite of density functionals for main group thermochemistry, thermochemical kinetics, noncovalent interactions, excited states, and transition elements: Two new functionals and systematic testing of four M06-class functionals and 12 other functionals. *Theor. Chem. Acc.* **2008**, *120*, 215–241. [[CrossRef](#)]
42. Hay, P.J.; Wadt, W.R. Ab initio effective core potentials for molecular calculations. Potentials for the transition metal atoms Sc to Hg. *J. Chem. Phys.* **1985**, *82*, 270–283. [[CrossRef](#)]
43. Elkodous, M.A.; El-Khawaga, A.M.; Maksoud, M.I.A.A.; El-Sayyad, G.S.; Alias, N.; Abdelsalam, H.; Ibrahim, M.A.; Elsayed, M.A.; Kawamura, G.; Lockman, Z.; et al. Enhanced photocatalytic and antimicrobial performance of a multifunctional Cu-loaded nanocomposite under UV light: Theoretical and experimental study. *Nanoscale* **2022**, *14*, 8306–8317. [[CrossRef](#)]
44. Abdelsalam, H.; Tebeb, N.; Wang, B.; Yunoki, S.; Zhang, Q. The electronic, adsorption, and catalytic properties of Bi-, Sb-, and As-nanoclusters. *Catal. Today* **2021**, *376*, 126–133. [[CrossRef](#)]
45. Wang, S.; Han, C.; Ye, L.; Zhang, G.; Hu, Y.; Li, W.; Jiang, Y. Electronic Properties of Triangle Molybdenum Disulfide (MoS<sub>2</sub>) Clusters with Different Sizes and Edges. *Molecules* **2021**, *26*, 1157. [[CrossRef](#)] [[PubMed](#)]
46. Gyorffy, B.L.; Pindor, A.J.; Staunton, J.; Stocks, G.M.; Winter, H.P. A first-principles theory of ferromagnetic phase transitions in metals. *J. Phys. F Met. Phys.* **1985**, *15*, 1337–1386. [[CrossRef](#)]
47. Wasilewski, B.; Marciniak, W.; Werwiński, M. Curie temperature study of Y(Fe<sub>1-x</sub>Co<sub>x</sub>)<sub>2</sub> and Zr(Fe<sub>1-x</sub>Co<sub>x</sub>)<sub>2</sub> systems using mean field theory and Monte Carlo method. *J. Phys. D Appl. Phys.* **2018**, *51*, 175001. [[CrossRef](#)]
48. Atkins, P.; Friedman, R. *Molecular Quantum Mechanics*; Oxford University Press: New York, NY, USA, 1997.
49. Cheeseman, J.R.; Trucks, G.W.; Keith, T.A.; Frisch, M.J. A comparison of models for calculating nuclear magnetic resonance shielding tensors. *J. Chem. Phys.* **1996**, *104*, 5497–5509. [[CrossRef](#)]
50. Bencini, A.; Totti, F. DFT description of the magnetic structure of polynuclear transition-metal clusters: The complexes [(Cu(bpca)<sub>2</sub>(H<sub>2</sub>O)<sub>2</sub>){Cu(NO<sub>3</sub>)<sub>2</sub>}]<sub>2</sub>, (bpca = Bis(2-pyridylcarbonyl)amine), and [Cu(DBSQ)(C<sub>2</sub>H<sub>5</sub>O)<sub>2</sub>], (DBSQ = 3,5-di-*tert*-butyl-semiquinonato). *Int. J. Quantum Chem.* **2004**, *101*, 819–825. [[CrossRef](#)]
51. Bencini, A.; Totti, F. A Few Comments on the Application of Density Functional Theory to the Calculation of the Magnetic Structure of Oligo-Nuclear Transition Metal Clusters. *J. Chem. Theory Comput.* **2009**, *5*, 144–154. [[CrossRef](#)] [[PubMed](#)]
52. Cui, S.X.; Wang, H.Y.; Xu, J.; Zhang, J.P. Theoretical studies on magnetic properties of a binuclear paddle wheel Cu(II) complex {Cu<sub>2</sub>( $\mu_2$ -O<sub>2</sub>CCH<sub>3</sub>)<sub>4</sub>}(OCNH<sub>2</sub>CH<sub>3</sub>)<sub>2</sub>. *Russ. J. Phys. Chem. A* **2017**, *91*, 1070–1075. [[CrossRef](#)]
53. Gusakova, J.; Wang, X.; Shiau, L.L.; Krivosheeva, A.; Shaposhnikov, V.; Borisenko, V.; Gusakov, V.; Tay, B.K. Electronic Properties of Bulk and Monolayer TMDs: Theoretical Study within DFT Framework (GVJ-2e Method). *Phys. Status Solidi (a)* **2017**, *214*, 1700218. [[CrossRef](#)]

**Disclaimer/Publisher’s Note:** The statements, opinions and data contained in all publications are solely those of the individual author(s) and contributor(s) and not of MDPI and/or the editor(s). MDPI and/or the editor(s) disclaim responsibility for any injury to people or property resulting from any ideas, methods, instructions or products referred to in the content.